GA–A23310

STATUS OF ADVANCED TOKAMAK SCENARIO MODELING WITH OFF-AXIS ELECTRON CYCLOTRON CURRENT DRIVE IN DIII–D

by
M. MURAKAMI, H.E. ST. JOHN, T.A. CASPER, M.S. CHU, J.C. DeBOO,
C.M. GREENFIELD, J.E. KINSEY, L.L. LAO, R.J. La HAYE Y.R. LIN-LIU, T.C. LUCE,
P.A. POLITZER, B.W. RICE, G.M. STAEBLER, T.S. TAYLOR, M.R. WADE,
AND THE DIII–D GROUP

DECEMBER 1999

DISCLAIMER

GA–A23310

STATUS OF ADVANCED TOKAMAK SCENARIO MODELING WITH OFF-AXIS ELECTRON CYCLOTRON CURRENT DRIVE IN DIII–D

by
M. MURAKAMI,* H.E. ST. JOHN, T.A. CASPER,† M.S. CHU, J.C. DeBOO, C.M. GREENFIELD, J.E. KINSEY,‡ L.L. LAO, R.J. La HAYE Y.R. LIN-LIU, T.C. LUCE,
P.A. POLITZER, B.W. RICE,† G.M. STAEBLER, T.S. TAYLOR, M.R. WADE,* AND THE DIII–D GROUP

This is a preprint of a paper to be presented at the 2nd IAEA Technical Committee Meeting on Steady-State Operation of Magnetic Fusion Devices, October 25–29, 1999, Fukuoka, Japan and to be published in the Proceedings

*Oak Ridge National Laboratory, Oak Ridge, Tennessee.
†Lawrence Livermore National Laboratory, Livermore, California.
‡Lehigh University, Bethlehem, Pennsylvania.

Work supported by
the U.S. Department of Energy
under Contract Nos. DE-AC03-99ER54463, DE-AC05-96OR22464, W-7405-ENG-48, and Grant No. DE-FG03-95ER54309

GA PROJECT 30033
DECEMBER 1999

ABSTRACT

The status of modeling work focused on developing the advanced tokamak scenarios in DIII–D is discussed. The objectives of the work are two-fold: (1) to develop AT scenarios with ECCD using time-dependent transport simulations, coupled with heating and current drive models, consistent with MHD equilibrium and stability; and (2) to use time-dependent simulations to help plan experiments and to understand the key physics involved. Time-dependent simulations based on transport coefficients derived from experimentally achieved target discharges are used to perform AT scenario modeling. The modeling indicates off-axis ECCD with approximately 3 MW absorbed power can maintain high-performance discharges with $q_{min} > 1$ for 5 to 10 s. The resultant equilibria are calculated to be stable to n = 1 pressure driven modes. The plasma is well into the second stability regime for high-n ballooning modes over a large part of the plasma volume. The role of continuous localized ECCD is studied for stabilizing m/n = 2/1 tearing modes. The progress towards validating current drive and transport models, consistent with experimental results, and developing self-consistent, integrated high performance AT scenarios is discussed.

1. INTRODUCTION

The key to sustaining the negative central shear (NCS) regime, the primary DIII–D Advanced Tokamak (AT) scenario [1], is maintenance of hollow current profiles using off-axis electron cyclotron current drive (ECCD). The EC system on DIII–D is being upgraded over the next few years from the present 3-gyrotron to a 6-gyrotron system for which more than 3 MW absorbed power is expected for long pulse operation in 2001. At the same time, multiyear experimental efforts are in progress to demonstrate AT plasma performance using off-axis ECCD. The goal is to achieve sustained, high normalized performance better than twice the conventional ELMing H–mode [product of normalized beta (β_N) and confinement enhancement factor relative to ITER89P scaling (H_{89P}) [2], $\beta_N H_{89P} \sim 10$] with a bootstrap current fraction (f_{bs}) exceeding 50%. The near-term goal has been transiently demonstrated in experiments using neutral beam injection (NBI) alone. The AT scenario modeling has used these target discharges to help address two major questions: (1) What is the scenario required to obtain optimum safety factor (q) and pressure profiles? (2) Can we maintain the desired profiles in steady state with the available EC power? The initial calculations used to guide the experimental effort were primarily based on "fixed profile scenarios" emphasizing MHD stability. In these scenarios, a total pressure profile consistent with an MHD stable equilibrium was rather arbitrarily divided into electron and ion pressures, which were then portioned to density and temperature. The purpose of the present studies is to use transport simulations to show such scenarios are achievable and help answer the above questions. The target discharge we pursue at this time is a high-performance ELMing H–mode discharge with NCS. A strong transport barrier near the boundary is subject to low-n kink modes associated with high edge current density. The repetitive ELMs provide a seed for neoclassical tearing modes and a region of high magnetic shear make neoclassical tearing modes unstable. The scenario modeling provides opportunities to study these challenging problems by simulating discharge conditions likely to be faced in the future.

In this paper, we first discuss ECCD scenario modeling based on existing NBI target discharges, specifically ELMing H–mode discharges with negative central shear (NCS) and then discuss stability aspects of ideal MHD stability and neoclassical tearing modes. Next, we discuss development toward a better scenario and AT physics studies. Here we discuss the time-dependent eqdsk mode (TDEM) of analysis and its applications to the determination of ECCD efficiency and the edge bootstrap current model. Lastly, we discuss a test of a theory-based model against experimental data from an impurity injection experiment.

1.1. SCENARIO MODELING USING ELMING H–MODE DISCHARGE CONDITIONS

The scenario modeling described here is based on transport coefficients determined from existing target discharges developed by the on-going experimental program on DIII–D. Simulations are carried out using the ONETWO time-dependent transport code [3], which is internally coupled with the TORAY ECH/ECCD ray tracing code [4]. Since recently developed target discharges (with NBI alone) satisfy the scenario target requirements, the transport coefficients [$\chi_e(\rho)$ and $\chi_i(\rho)$] calculated from these target discharges can be directly used as the baseline model for the time-dependent transport simulations. When the target plasma parameters for the simulations are different from those of the target discharges, the transport coefficients were scaled based on the ITER89P scaling expression [2] while leaving the profiles of transport coefficients unchanged [5].

Figure 1 shows characteristics of a high performance ELMing H–mode (β_N = 3.5, H_{89P} = 2.8, and q_{95} = 5.0) target discharge with double-null divertor pumping. The cryopumping kept the line-average electron density ($\bar{n}_e = 4.8 \times 10^{19}$ m^{-3}) about 20% lower than that without pumping, although this density value is not the lowest that has been achieved with pumping. Figure 2 shows profiles of the electron temperature (T_e), ion temperature (T_i) and electron density (n_e) of this target discharge together with calculated electron and ion thermal diffusivities, $\chi_e(\rho)$ and $\chi_i(\rho)$, based on a power balance analysis.

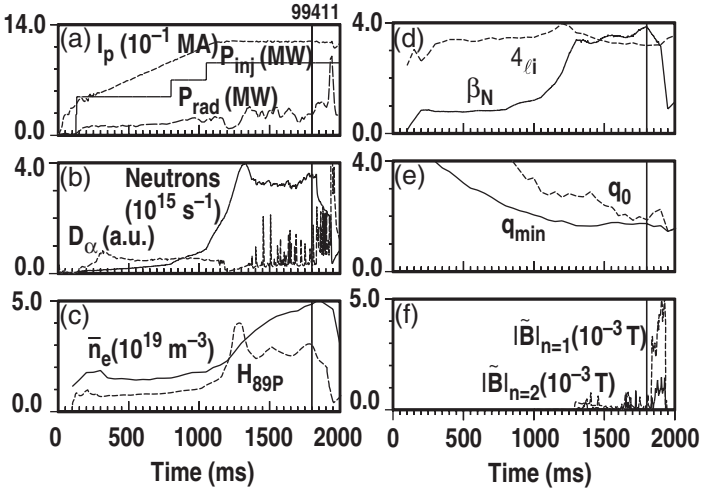

Fig. 1. Time evolution of a high performance ELMing H–mode discharge with cryopumping. This shot reached β_N = 3.7, H_{89P} = 2.8, and the product $\beta_N H_{89P}$ = 10 for about 2 τ_E. The calculated bootstrap current is 55% of the total current, I_p = 1.2 MA at B_T = 1.6 T with q_{95} = 5.0. The vertical line at t = 1800 ms shows when the simulations were began. The high performance phase was terminated at the onset of neoclassical tearing mode (m/n = 2/1) activity.

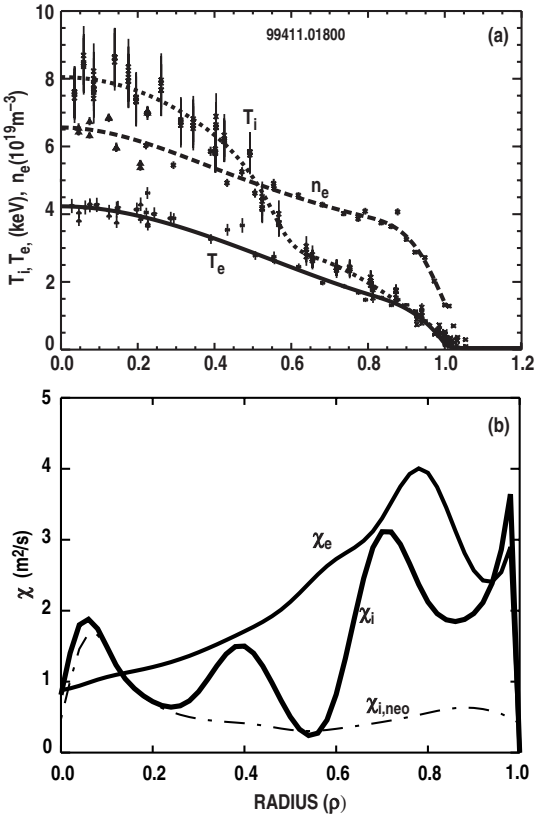

Fig. 2. Thermal diffusivities calculated from the initial profiles of ion and electron temperature and electron density.

Simulations of an AT discharge with ECCD are based on the above target discharge. We replace a part of the NBI power with off-axis ECH/ECCD power so that the total input power is kept constant. The EC launching direction is optimized to sustain the high performance. The TORAY code carries out the ray tracing for ECH power deposition. The oblique launching angle is adjusted for the refractive effect due to the strong density gradient at the plasma edge. The code calculates the current drive by taking into account the trapped electron effects. Figure 3 shows the normalized (local) ECCD efficiency ($\varsigma = 33 \bullet n_{20} I_A R_m / P_W T_{kev}$) as a function of the normalized minor radius of the EC resonance location. The decrease in the calculated efficiency as we move further off-axis is due to the trapped electron effect. However, as discussed later, the experimentally measured current drive efficiency does not decrease as much with radius as calculated from theory [6]. On that account, the present simulations are based on a conservative estimate of off-axis ECCD efficiency. Based on the ECCD calculated, the ONETWO code solves the current diffusion equation self-consistently with the fix boundary MHD equilibrium. The radial location of the current drive substantially affects the time when a $q_{min} = 1$ surface appears in the plasma. Since avoiding the m/n = 1/1 sawtooth instability is a necessary condition for achieving high performance, EC optimization by varying the resonance location was done to maximize the duration before $q_{min} = 1$ is reached. The simulation

with off-axis ($\rho \sim 0.5$) ECCD with 3 MW power shows that ECCD can sustain an enhanced confinement condition ($\beta_N H_{89P} \sim 9$) at $\beta_N = 3.5$ and $H_{89P} = 2.6$ with bootstrap current fraction (f_{bs}) of 55% for more than 10 s which is about twice the skin time.

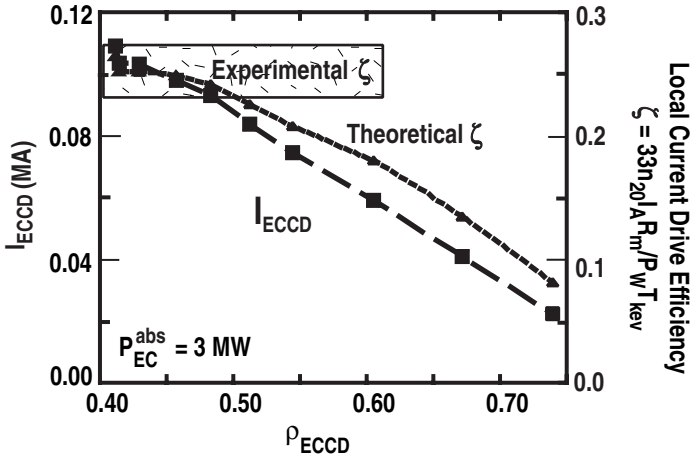

Fig. 3. EC driven current and (local) current drive efficiency calculated by the TORAY code as a function of the normalized EC resonance radius. The experimental results of the current drive efficiency show little decrease with radius.

Figure 4 shows the safety factor $q(\rho)$ and total pressure profiles at the end of a 10 s compared with the initial state and individual components of the current profile for this case. MHD stability calculations show that, with no wall, the equilibrium is unstable to a global n = 1 pressure driven mode. With a conducting wall at 1.5 times minor radius, it is found to be stable to the ideal n = 1 mode. Ballooning stability calculations show that the core is well into the second ballooning stability regime over a large part of the plasma volume. In this discharge simulation, the $q(\rho)$ profile remains inverted in the core for about 1 s and, thereafter, the magnetic shear remains weakly positive with q(0) slowly dropping. Ideal MHD stability studies of the impact of varying the $q(\rho)$ profiles with corresponding pressure profiles indicated that the NCS q-profile has little effect on ideal low-n pressure-driven modes. The next concern is nonideal MHD stability, in particular, resistive wall modes [1,7] and neoclassical tearing modes. Since the target discharge (without ECCD) suffered from m/n = 2/1 tearing mode activity shortly after the simulation initiation time [Fig. 1]. However, usual high-performance target discharges are not limited by tearing modes.

Continuous localized ECCD can stabilize neoclassical tearing modes (NTM). Experimentally, NTMs tend to develop at the lowest m–mode rational surfaces to a given n-number (*i.e.*, m/n = 3/2, 2/1, and 4/3) for which Δ' tends to be least negative [8], where Δ' is the logarithmic jump in poloidal flux across the tearing layer at the singular surface (r_s). We focus here on the stability of an m/n = 2/1 tearing mode with $q_{min} > 1.5$. Since

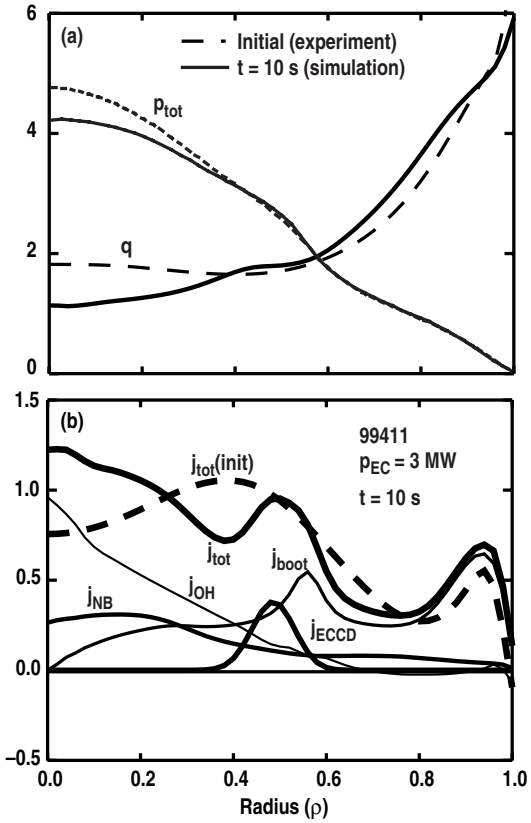

Fig. 4. Comparison of the initial and final safety factor and total plasma pressure profiles and individual current density components after 10 s.

calculation of the tearing instability parameter Δ' is rather involved, we adopt an approximate tearing instability parameter [9],

$$\lambda = \frac{rq}{m(dq/dr)} \frac{\mu_0}{B_\theta} \left(-\frac{dJ_\parallel}{dr} \right)\Bigg|_{r=r_s} ,$$

evaluated at the rational surface. This parameter is derived in the limit for circular flux surfaces in a cylinder and ignores the toroidal coupling: This approximation needs to be benchmarked with more accurate Δ' calculated by PEST–3 [10]. The stability of tearing modes is inversely related to λ. Figure 5 shows the contour plot of the product of the poloidal mode number (m) and the tearing instability parameter λ for the simulation case with ECCD at ρ = 0.61. Figure 6 shows the radial dependence of q(ρ) and $J_\parallel$(ρ) for several different times in the simulation. This indicates that small positive or negative λ (and thus negative Δ') can be maintained with continuous localized ECCD. Table I shows the corresponding calculations of PEST–3 for Δ', indicating the λ behavior is in rather good agreement with that of Δ'. As suggested by Pletzer [11], when co-ECCD is applied just outside the q = 2 location, stability is improved. Even when the mode is conventionally stable ($\Delta' < 0$), the perturbed neoclassical bootstrap current can induce

destabilization if β_θ exceeds a critical value and the rational surface is sufficiently perturbed (for example, by ELMs). Figure 7 shows the calculated critical poloidal beta (β_θ) diagram from the modified Rutherford equation [8] as a function of normalized island width for several $\Delta' r_s$. The 2/1 NTM is predicted to be completely stable at the experimental β_θ (=1.8) for any size perturbation with large enough negative $\Delta' r_s$.

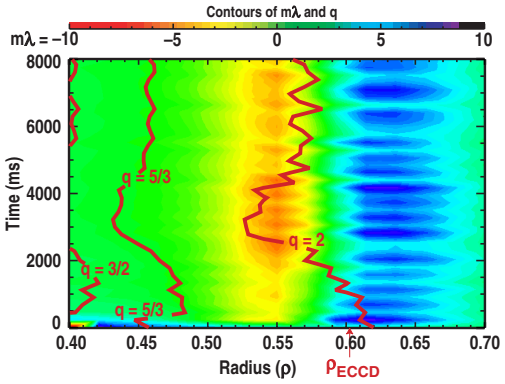

Fig. 5. Contour plots of mλ (product of the poloidal mode number and the approximate tearing instability parameter) and rational surfaces (q=2, 3/2, and 4/3) for the simulation case with $\rho_{ECCD} = 0.61$.

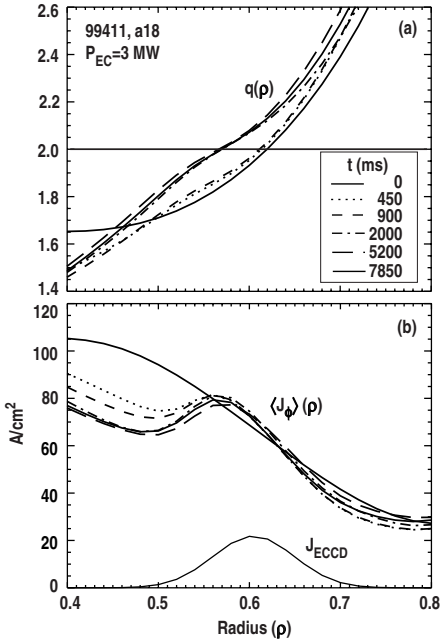

Fig. 6. Profiles of safety factor and flux-averaged toroidal current at several different times during the simulation with ECCD localized at ρ = 0.61. As seen in Table I (PEST–3), continuous localized ECCD stabilization of tearing modes ($\Delta' < 0$) is more effective when ECCD is outside the q=2 surface.

Table I
The q=2 Resonance Surface Location and Tearing Mode Instability Parameters, λ and $\Delta' R_S$, the Latter Calculated by the PEST–3 Code, for M/N = 2/1 Tearing Mode

t (ms)	$r_{q=2}$	l(q=2)	$\Delta' r_s$
450	0.620	0.620	+127
1550	0.614	2.413	+48
2000	0.570	0.335	–85
5200	0.560	–0.567	–1580
7850	0.570	–0.570	+1.5

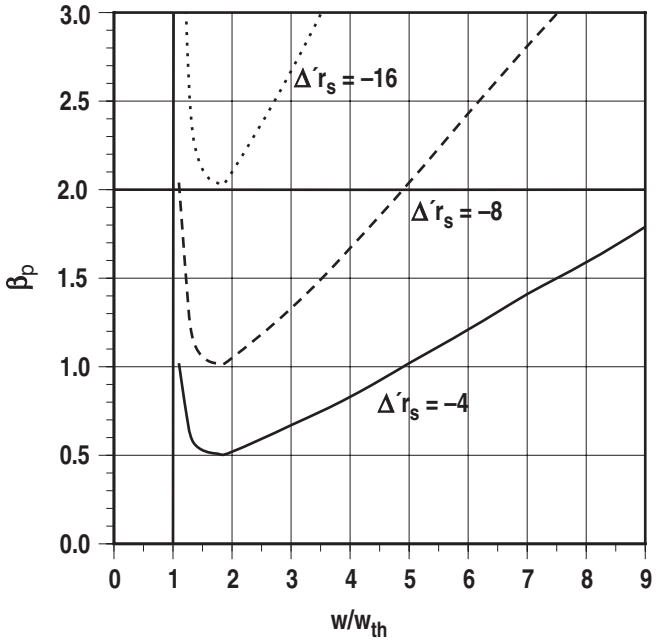

Fig. 7. Critical poloidal beta as a function of normalized island width of neoclassical tearing modes for several values of $\Delta' r_s$. For each value of $\Delta' r_s$, the curve on the left side of the minimum gives the seed island width, while the right side curve gives the saturated island width. The 2/1 NTM is predicted to be completely stable for a large enough (stable) $|\Delta' r_s|$ value, i.e., all seed islands are too small to sufficiently perturb the metastable plasma.

2. PROGRESS TOWARDS DEVELOPING SELF-CONSISTENT AT SCENARIO MODELING

Scenario modeling to date [3] showed that ~3 MW EC power is sufficient to sustain the high performance for 5 to 10 s by keeping $q_{min} > 1$ which is essential to avoid detrimental sawtooth oscillations. However, the NCS feature in the q-profile vanishes rather quickly at the beginning of the simulation and remains weakly positive for most of the time. It proved to be difficult to make a smooth transition from the target (NBI) phase to ECCD simulation phase, primarily for two reasons: Ohmic current residue and a transient inductive response to the application of ECCD.

The Ohmic current profile plays a significant role in determining the q-profile. In the usual predictive simulations, Ohmic current is determined by subtracting all noninductive current components from the total current, $J_{OH} = J_{tot} - (J_{bs} + J_{NB} + J_{ECCD})$. Therefore, all noninductive current drive must be correct if the Ohmic current is to be correct. On the other hand, thanks to the advent of relatively new diagnostics, in particular, space and time resolved motional Stark effect (MSE) diagnostics and "kinetic" profile diagnostics (including Z_{eff} measurement), the Ohmic current profile is probably the most well-known current component in the experimental (data) analysis phase. The predictive simulation should take advantage of the known OH current (or internal loop voltage) information. Once an unwanted J_{OH} is excited, it takes a long time to dissipate. CD startup transients tend to perturb $q(\rho)$ due to "back EMF," but a slow CD ramp [12] is not practical because of a limited pulse length available. Therefore, the real challenge is how to make a smooth transition from the data analysis phase to the predictive simulation phase. The internal loop voltage behavior is the key in this transition.

The time-dependent eqdsk mode (TDEM) [13] of simulation in ONETWO simulation uses the geometry and inductively driven source terms. The latter information is extracted in the same manner as the CD determination technique developed by Forest [14]. The TDEM allows us to use a series of experimentally derived MHD equilibria (eqdsk) to generate the space- and time-dependent coefficients required in confinement analysis. Although it is still a challenge to feed the internal loop voltage information forward to the simulation phase, this TDEM helps carry out internal loop voltage analysis during the experimental data analysis phase within the same transport code. Along this line, we describe two examples of the TDEM application: determination of ECCD and edge current profile evolution, both of which will help to verify the noninductive current drive models. These topics are also very relevant to the AT physics studies.

The TDEM approach for determining ECCD is benchmarked well with the internal loop voltage analysis of ECCD [6] carried out by the stand-alone code, NVLOOP [15]. The poloidal flux, $\Psi(\rho,t)$ is given by a series of equilibrium reconstructions with a fine

time resolution based on the MSE diagnostic and magnetic measurements incorporated with pressure profiles. The total current is given by spatial derivatives of Ψ, while the Ohmic current J_{OH} is given by $\sigma_{neo}E_{||}$, where σ_{neo} is the neoclassical conductivity and $E_{||}$ is the parallel electric field determined by the time derivative of Ψ. The noninductive current can be calculated by subtracting the Ohmic current from the total current. Comparison of a ECCD+NBI case with a NBI-only case allows one to separate ECCD from NBCD and bootstrap current. This process was applied to an off-axis ECCD case [6] within the ONETWO code. Figure 8(a) shows the noninductive current density J_{NI} for the ECCD+NBI case compared with the NBI-only case. Figure 8(b) shows the ECCD components obtained by subtraction. This result agrees well with the ECCD that was carried out with NVLOOP analysis [15]. (The latter analysis applied an additional correction for changes in the kinetic profiles and neutral beam power near the axis.) The area integral of the ECCD yields a value substantially larger than the theoretically calculated value (35 kA versus 8 kA). The inferred ECCD profile is also broader than that predicted by theory. The broadening appears to be the result of finite spatial resolution of the present equilibrium reconstruction technique [16].

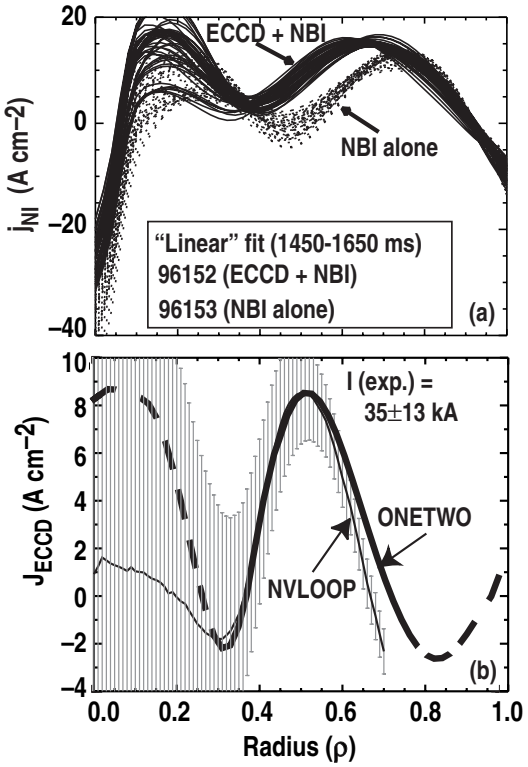

Fig. 8. (a) The radial profile of the noninductive current density (J_{NI}) for off-axis ECCD (solid line) and NBI-only (dashed line) calculated in the ONETWO code. (b) The profiles of the ECCD current density calculated by the ONETWO code is compared with the stand-alone NVLOOP code.

Another application of the TDEM technique is edge current profile evolution. Control of edge stability is a key step toward extending the duration of AT modes. The improved confinement from an edge transport barrier tends to result in large pressure gradients (p') and large edge currents (J_{edge}), which often drive MHD instabilities that can terminate the discharge or reduce the performance. The pressure gradient and bootstrap current work in a positive feedback loop, which allows second stability access in the edge. Removing the second stability access will reduce the edge p' and amplitude of ELM perturbations [17]. Reducing the edge current should be favorable since this will reduce the kink-like character of the edge instability. A key question is how large the edge current is, relative to that driven by the bootstrap current. This issue has been addressed by comparison between the experimental analysis (TDEM) and the bootstrap model simulation. The former computes the current density from a series of reconstructed equilibria with a fine time resolution (5 ms), while the latter solves the current diffusion equation with bootstrap current calculated from detailed edge pressure gradients ("kinetic" profiles) based on the NCLASS model [17]. Figure 9(a) shows deuterium Balmer light (D_α) from a high performance discharge in which the L–mode transitions to ELM-free H–mode, followed by a series of ELMs. The TDEM analysis [Fig. 9(b)] shows the edge current at ρ = 0.95 rises quickly after the L–H transition, while the inductive response of the plasma ("back EMF") drives current negative just inside this region. Comparison between the TDEM analysis and the bootstrap simulation [Fig. 9(c)] indicates that the experimentally observed current is 30% to 50% lower than the bootstrap current. However, further work is needed to make this conclusion more concrete on both experimental and theoretical sides. In the experimental analysis, sensitivity studies need to be done in the equilibrium reconstruction. In the bootstrap simulation, the edge bootstrap current model needs to be improved since this model (for that matter, all bootstrap models) has not incorporated the effect of trapped particle orbit loss at the edge. The simulations shown in Fig. 10 indicate that some control of the edge current can be obtained by changing Z_{eff}

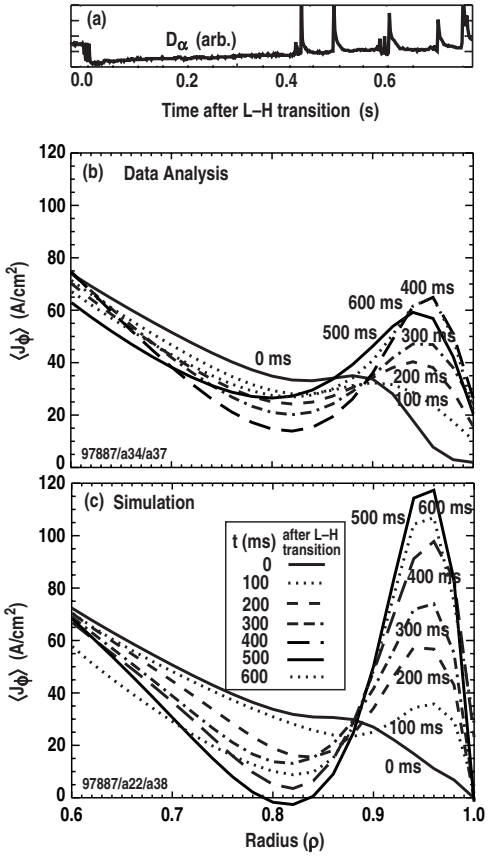

Fig. 9. Comparison of edge current density profiles in: (b) the experimental analysis and (c) the bootstrap model simulation at several different phases of the H–mode discharge after L–H transition (as shown by the D_α signal). The discharge conditions (97887.2405) are: I_p = 1.5 MA, B_T = 2.1 T, $n_e = 5.4 \times 10^{19}$ m^{-3}, and P_{inj} = 7.4 MW.

(edge collisionality) with impurity injection. Precision measurements of edge current with sufficient space and time resolution are planned by developing the Zeeman polarimetry diagnostic with a lithium-beam on DIII–D.

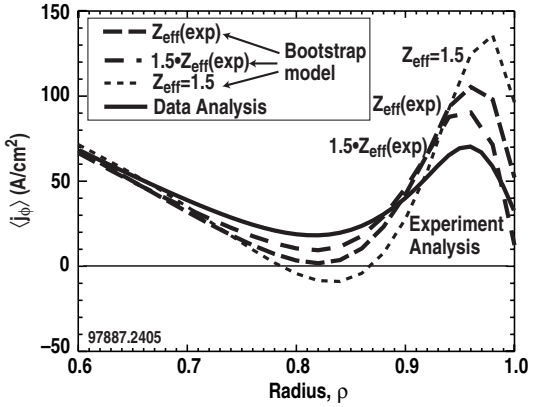

Fig. 10. Effects of changing the effective-Z (Z_{eff}) on the edge current density profiles in the bootstrap model simulation. The experimental Z_{eff} profile has $Z_{eff} \approx 3$ at $\rho = 0.6$ to 0.95.

Full exploitation of profile optimization needs comprehensive theory-based predictive transport models. Since simulations to date in ONETWO have used a transport model based on fixed (in time) experimentally measured density profiles and fixed thermal diffusivities calculated from experiments, they cannot reproduce the dynamics of a transport barrier formation and temporal evolution. In addition, assessing the effect of the q-profile and magnetic shear on transport properties is an important subject that requires experimental and theoretical study. We are in the process of incorporating the gyro-Landau-fluid GLF23 model [19] into the ONETWO transport code [20]. This model includes magnetic shear and E×B flow shear effects on ion, electron, particle transport, and momentum transport. This code needs to be tested against some experiments.

One experiment suitable for this purpose is the impurity injection experiment [21] performed on DIII–D where clear increases in confinement ($H \leq 2$) and reductions of long-wavelength turbulence have been observed which are directly correlated with external impurity (Ne, Ar, Kr) injection in L–mode discharges. The GLF23 model is used to solve the V_ϕ, T_i, and T_e equations with the experimental $n_e(\rho)$ profile and boundary conditions at $\rho = 0.8$. The GLF23 model includes the effects of toroidal drift wave turbulence and E×B shearing on transport. Two simulations are shown in Fig. 11: experimental $Z_{eff}(\rho)$, and $Z_{eff} = 1.5$ with carbon alone. The model shows that both E×B shearing and growth rate reduction due to impurity are needed to explain the observed confinement improvement.

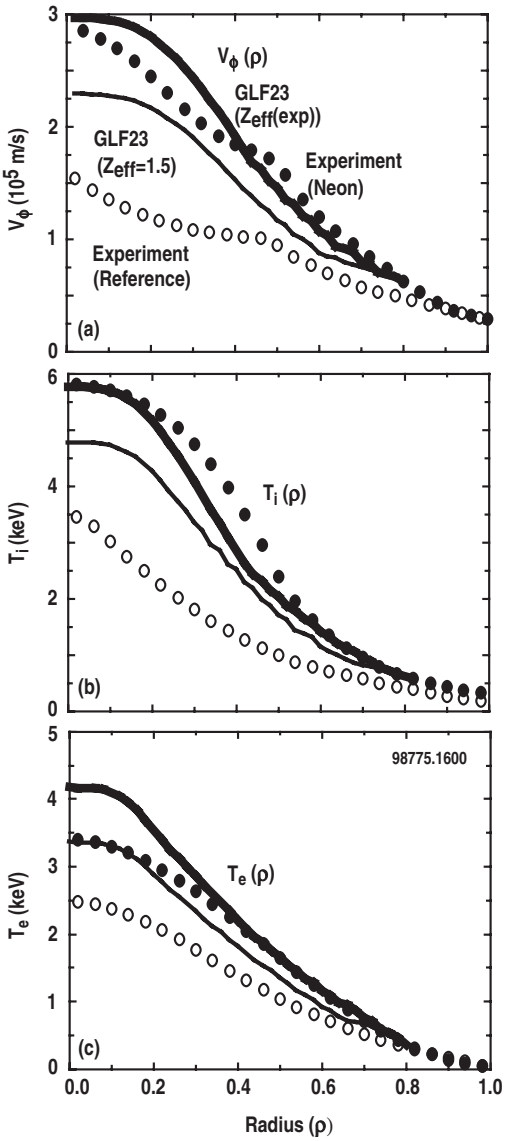

Fig. 11. Profiles of toroidal velocity, ion temperature, and electron temperature from the GLF23 model with two different Z_{eff} profiles [experimental profile ($Z_{eff} \approx$ 3 with neon), and Z_{eff} = 1.5 (constant with carbon)] at the end of the simulation compared with the experimental profiles (solid points). The impurity injection (shot 98775) resulted in significant increases in V_f, T_i, and T_e, compared with those in the reference shot (Shot 98777, shown by open points).

3. CONCLUSIONS

The status of modeling work focused on developing self-consistent, integrated high-performance AT scenarios, and validating current drive and transport model, consistent with experimental results have been discussed. Time-dependent simulations based on transport coefficients derived from experimentally achieved target discharges are used to perform AT scenario modeling. Off-axis ECCD with approximately 3 MW absorbed power can maintain high-performance discharges with $q_{min} > 1$ for 5 to 10 s which is $(1 – 2) \times \tau_{skin}$. The resultant equilibria are calculated to be stable to n = 1 pressure driven modes. The plasma is well into the second stability regime for high-n ballooning modes over a large part of the plasma volume. The role of continuous localized ECCD was studied for stabilizing m/n = 2/1 tearing modes. The challenge is to make a smooth transition from the experimental data analysis phase to the predictive simulation phase. Utilizing estimates of internal loop voltage is a key for obtaining a smooth transition. Several noninductive current drive models need to be verified against experiments. Along this line, we have utilized TDEM (or internal loop voltage) analysis for computing off-axis ECCD efficiency, and edge current profile evolution to compare with bootstrap current model. In the future, we need a comprehensive theory-based transport model for modeling ITB dynamics. The GLF23 model is being implemented in ONETWO and tested against experiments.

ACKNOWLEDGMENTS

The authors would like to thank the DIII–D Team for their contributions to this work. This is a report of work supported by the U.S. Department of Energy under Contract Nos. DE-AC03-99ER54463, DE-AC05-96OR22464, W-7405-ENG-48, and Grant No. DE-FG03-95ER54309.

REFERENCES

[1] Chan, V.S., *et al.*, "DIII–D Advanced Tokamak Research Overview," to be published in Proc. 2nd IAEA Tech. Com. Mtg. on Steady State Operation of Magnetic Fusion Devices, October 25–29, 1999, Fukuoka, Japan; General Atomics Report GA–A23312 (1999).

[2] Yushimanov, P.N., Nucl. Fusion **30** (1990) 1999.

[3] St. John, H.E., *et al.*, Proc. 15th Int. Conf. on Plasma Physics and Controlled Nuclear Fusion Research, Seville, Vol. 3, p. 603 [International Atomic Energy Agency, Vienna, (1995)].

[4] Matsuda, K., IEEE Trans. Plasma Sci. **17** (1989) 6.

[5] Murakami, M., *et al.*, Proc. 26th European Conf. on Controlled Fusion and Plasma Physics, Maastricht, Vol. 23J, p. 1213 (European Physical Society, 1999).

[6] Luce, T.C., *et al.*, "Generation of Localized Non-Inductive Current by Electron Cyclotron Waves on the DIII–D Tokamak," to be published in Phys. Rev. Lett.; General Atomics Report GA–A23018 (1999).

[7] Garofalo, A.M., *et al.*, "Control of the Resistive Wall Mode in Advanced Tokamak Plasmas on DIII–D," 2nd IAEA TCM on Steady-State Operation of Magnetic Fusion Devices, October 25–29, 1999, Fukuoka, Japan, submitted to Nucl. Fusion; General Atomics Report GA–A23272 (1999).

[8] La Haye, R. J., and Sauter, O., Nucl. Fusion **38** (1998) 987.

[9] Hegna, C.C., and Callen, J.D., Phys. Plasmas **1** (1994) 2308.

[10] Pletzer, A., Bondeson, A., and Dewars, R.L., J. Comput. Phys. **115** (1994) 530.

[11] Pletzer, A., and Perkins, F.W., Phys. Plasmas **6** (1999) 1589.

[12] Moreau, D., and Voitsekhovitch, I., Nucl. Fusion **39** (1999) 685.

[13] St John, H.E., *et al.*, Bull. Am. Phys. Soc. **41** (1996) 1571.

[14] Forest, C.B. *et al.*, Phys. Rev. Lett. **73** (1994) 2444.

[15] Politzer, P.A., private communication (1999).

[16] Luce, T.C., *et al.*, "Determination of the Electron Cyclotron Current Drive Profile," to be published in Proc. 11th Workshop on Electron Cyclotron Emission and Electron Cyclotron Resonance Heating, Oharai, Japan, October 1999; General Atomics Report GA–A23259 (1999).

[17] Osborne, T.H., *et al.*, J. Nucl. Mater. **266–269** (1999) 131.

[18] Houlberg, W.A., *et al.*, Phys. Plasmas **4** (1997) 3230.

[19] Waltz, R.E., *et al.*, Phys. Plasma **4** (1997) 2482.

[20] Kinsey, J.E., *et al.*, Proc. 26th European Conf. on Controlled Fusion and Plasma Physics, Maastricht, Vol. 23J, p. 1205 (European Physical Society, 1999).

[21] McKee, G.R., "Impurity-Induced Core Turbulence Suppression and Reduced Transport in the DIII–D Tokamak," presented at 41st Am. Phys. Soc. Annual Meeting of the Division of Plasma Physics, November 15–19, 1999, Seattle, Washington, to be published in Phys. Plasmas; General Atomics Report GA–A23300 (to be printed).